

This manuscript is a preprint and has been submitted for publication in Nature Communications. It has not yet been peer-reviewed. Subsequent versions of this manuscript are likely to differ as a result of feedback from reviewers and preprint readers. If accepted for publication, the final version will be available via the “Peer-reviewed publication DOI” link on EarthArXiv. We hope you find this paper interesting and would welcome your feedback on it.

Please contact Nanna B. Karlsson (nbk AT geus.dk) with your feedback or questions.

Title: A First Constraint on Basal Melt-water Production of the Greenland Ice Sheet

Authors: Nanna B. Karlsson^{1,*}, Anne M. Solgaard¹, Kenneth D. Mankoff¹, Fabien Gillet-Chaulet², Joseph A. MacGregor³, Jason E. Box¹, Michele Citterio¹, William T. Colgan¹, Kristian K. Kjeldsen¹, Niels J. Korsgaard¹, Douglas I. Benn⁴, Ian Hewitt⁵, and Robert S. Fausto¹

Affiliations:

1 Geological Survey of Denmark and Greenland, Copenhagen, Denmark

2 University of Grenoble Alpes, CNRS, IGE, Grenoble, France

3 Cryospheric Sciences Laboratory, NASA Goddard Space Flight Center, Greenbelt, Maryland, USA 10

4 School of Geography & Sustainable Development, University of St. Andrews, St. Andrews, UK

5 Oxford Centre for Industrial and Applied Mathematics, University of Oxford, Oxford, UK

A First Constraint on Basal Melt-water Production of the Greenland Ice Sheet

Nanna B. Karlsson^{1,*}, Anne M. Solgaard¹, Kenneth D. Mankoff¹, Fabien Gillet-Chaulet², Joseph A. MacGregor³, Jason E. Box¹, Michele Citterio¹, William T. Colgan¹, Signe H. Larsen¹, Kristian K. Kjeldsen¹, Niels J. Korsgaard¹, Douglas I. Benn⁴, Ian J. Hewitt⁵, and Robert S. Fausto¹

¹Geological Survey of Denmark and Greenland, Copenhagen, Denmark

²University of Grenoble Alpes, CNRS, IGE, Grenoble, France

³Cryospheric Sciences Laboratory, NASA Goddard Space Flight Center, Greenbelt, Maryland, USA

⁴School of Geography & Sustainable Development, University of St. Andrews, St. Andrews, UK

⁵Oxford Centre for Industrial and Applied Mathematics, University of Oxford, Oxford, UK

*Corresponding author: nbk@geus.dk

The Greenland ice sheet has been one of the largest sources of sea-level rise since the early 2000s. However, basal melt has not been included explicitly in assessments of ice-sheet mass loss so far. Here, we present the first estimate of the total and regional basal melt produced by the ice sheet and the recent change in basal melt through time. We find that the ice sheet's present basal melt production is $21.4 \pm 4.4/-4.0$ Gt per year, and that melt generated by basal friction is responsible for about half of this volume. We estimate that basal melting has increased by 2.9 ± 5.2 Gt during the first decade of the 2000s. As the Arctic warms, we anticipate that basal melt will continue to increase due to faster ice flow and more surface melting thus compounding current mass loss trends, enhancing solid ice discharge and modifying fjord circulation.

25 Introduction

26 Mass loss from the Greenland ice sheet is determined via one of three methods: through estimates
27 of ice volume change from satellite altimetry[1, 2], by measuring changes in regional gravity[3]
28 or by differencing between solid ice discharge and surface mass balance[4, 5] (the “input–output”
29 method, the term solid ice discharge refers to the ice volume that exits through flux gates at the
30 margin). Presently, the average mass balance of the ice sheet is -254 ± 18 Gt per year (average
31 over 2005-2015) with a spread between different mass balance estimates of 36 Gt per year [6].
32 Gravity methods implicitly include basal mass loss, while altimetry methods attribute all mass
33 loss to either ice discharge or surface mass loss. Either method provides limited insights into the
34 physical processes leading to the observed change in mass. In contrast, the input-output method
35 relies on accurate process representation of the different mass-loss terms and thus provides the
36 possibility of predicting future changes. To date, the input-output method has overlooked basal
37 mass balance entirely. Constraining basal melt is important for three reasons. Firstly, uncertainty
38 in the partition of ice-sheet mass loss between surface mass balance and ice discharge, including
39 the failure to acknowledge the basal mass balance term, limits our understanding of changes in
40 ice-sheet mass budget in response to recent climate change. This impedes our ability to capture
41 complex interactions and feedbacks between ice sheets and the climate system. Secondly, recent
42 studies have highlighted the importance of subglacial discharge for modifying the mass loss from
43 marine-terminating glaciers. Subglacial discharge increases the total submarine melt flux [7, 8]
44 and plays an important role for Greenland outlet glaciers’ contribution to future sea-level rise[9,
45 10]. Finally, discharge of subglacial water modifies circulation in the fjord systems and may impact
46 nutrient mixing[11, 12].

47 Here, we provide the first estimate of ice-sheet-scale basal melt and its change through the
48 first decade of the 2000s. We consider three sources of basal heat that generate melt (Fig. 1A-C).
49 The first source, the geothermal flux, is assumed to be constant in time while the other terms,
50 frictional heat and heat from surface melt water, vary in response to changes in ice dynamics
51 and surface melt. We quantify the basal melt using estimates of geothermal flux, satellite-derived
52 ice-surface velocities, surface and bed topographies, and outputs from regional climate models.
53 We use a multi-year surface velocity composite spanning 1995-2015[13], as well as winter veloc-
54 ity maps from 2000/2001 to 2018/2019[14, 15], and average surface melt-water volumes from
55 1991-2012[16]. This allows us to construct a baseline basal-melt value against which we can com-
56 pare likely changes in basal melt rates in the recent past. We assume that all basal melt water
57 is discharged to the ocean since the geometry and high surface slopes of the ice sheet preclude
58 the existence of large subglacial lakes[17]. Although studies have found evidence of subglacial
59 lakes[18, 19] and “units of disturbed radio-stratigraphy” [20, 21], associated volumes are negligi-
60 ble in the context considered here. Similarly, model results indicate that basal freeze-on rates are
61 unlikely to be of significance for the basal mass budget[22]. Our results demonstrate that basal

62 melt is a non-negligible component of the mass balance of the Greenland ice sheet, and that basal
63 melt-water production is likely increasing and will continue to do so in the foreseeable future.

64 **Results**

65 **Geothermal flux contribution to basal melt**

66 The heat from the geothermal flux is based on an average of three geothermal flux maps[23, 24, 25]
67 and is masked with an independent estimate of where basal ice is likely at pressure melting
68 point[26] (Fig. 1A, black and grey contours). Our estimate of total geothermal basal melt is
69 $5.3+2.8/-2.2$ Gt per year (Table 1, note that our uncertainty range is asymmetrical and we use
70 ‘/’ to denote upper/lower range). The uncertainty is due to the embedded uncertainties in the
71 geothermal flux estimates as well as the unknown basal temperature of the ice. We find that the
72 difference in ice-sheet-wide basal melt between the geothermal datasets is $< 10\%$, however, by
73 including the likely range of geothermal flux based on each dataset’s stated uncertainty, the final
74 uncertainty range increases (see methods). Studies suggest that the geothermal flux is generally
75 underestimated in the northeastern (NE) sector due to the presence of a localised “hot spot” under
76 the North East Greenland ice stream[27, 28]. Therefore, our estimate comes with the caveat that
77 the contribution from the NE sector is likely larger than the estimate presented here.

78 Spatially, the basal melt caused by geothermal flux is evenly distributed (Fig. 1 D). The highest
79 melt rates are found in the central eastern (CE) sector where basal melt in a few places exceeds
80 10^{-2} m per year. In the CE, SW (southwestern) and SE (southeastern) sectors, melt rates are typi-
81 cally 6-7 mm per year, while melt rates for the remaining sectors are 5 mm per year or less. There
82 is no contribution to the geothermal basal melt in the interior of the ice sheet, where basal ice
83 temperatures are likely below the pressure melting point[26].

84 **Frictional heat contribution to basal melt**

85 The frictional heat is produced by ice sliding over the bed. We retrieve an estimate of the frictional
86 heat using the Elmer/Ice model, where the complete stress balance is solved (“Full Stokes”) [29],
87 and where basal sliding and shear stress are related by a linear friction law[30]. Using the present
88 day topography, the spatially-varying friction coefficient is tuned to reproduce the observed sur-
89 face velocities (Fig. 1B). Thus, the model returns an estimate of basal frictional heating, constrained
90 by surface observations. From this heat estimate we get the resulting basal melt (see methods) and
91 we apply the same mask of basal conditions as used in the geothermal flux calculation[26]. Note
92 that the Elmer/Ice output does predict basal melt under most of the ice sheet although the basal
93 melt rates are orders of magnitude smaller in masked areas compared to melt rates predicted
94 along the margins. We find that the total basal melt due to frictional heat is 10.9 ± 2.9 Gt per year

95 (see methods for a discussion of uncertainties).

96 Melt from frictional heating is concentrated in areas with high ice-flow velocities i.e. at major
97 glacier outlets (Figs. 1B and E). Most of the basal melt water is drained through large ice streams
98 and several of the major outlets have melt rates orders of magnitude above the melt rates produced
99 by the geothermal flux. In the slow-flowing interior, friction melt rates are typically at least an
100 order of magnitude lower. In the northern (NO) sector, the outlet of Petermann Gletsjer is visible
101 as an extended area where friction melt exceeds 10^{-2} m per year. Near the margin, melt rates
102 approach and exceed 0.3 m per year. In the NE sector, most of the friction melt is generated by
103 Nioghalvfjærdsfjorden glacier and Zachariae Isstrøm, and rates exceed 0.2 m per year close to the
104 margin. High friction melt rates are also found in the CE and SE sectors where Kangerlussuaq
105 Glacier and Helheim Glacier cause friction melt in excess of 0.3 m per year. In these three sectors,
106 friction melt rates exceeding 10^{-2} m per year extend inland. Basal friction as a source of melt is less
107 important in the slow-flowing sectors. In the predominantly land-terminating southwestern (SW)
108 sector, friction melt does not exceed 0.2 m per year except in a few grid cells by the ice margin. The
109 central western (CW) sector has the largest areal extent of high friction melt rates and undergoes
110 melt rates above 0.4 m close to the margin in several places. High friction melt in the CW sector
111 is in part due to Sermeq Kujalleq (Jakobshavn Isbræ), one of Greenland's largest outlet glaciers.
112 In contrast, the northwestern (NW) sector contain numerous smaller glaciers but combined they
113 also create a large area where melt rates exceed 10^{-2} m per year.

114 **Surface melt water heat contribution to basal melt**

115 Finally, we consider the heat generated by surface melt water as it infiltrates the subglacial sys-
116 tem (Fig. 1C), and we convert the gravitational potential energy of surface melt water into heat,
117 which melts open subglacial conduits as water flows through the ice sheet, assuming that all water
118 reaches the bed. We further assume that the water only penetrates to the bed at altitudes below
119 2000 m above sea level. This heat source has been calculated in previous studies[31] using surface
120 water volumes from a regional climate model[32] but not translated directly into basal melt rates.
121 Here, we use a recently published surface melt-water estimate based on an average of 13 regional
122 climate models[16]. We estimate that the average basal melt due to surface melt-water injection
123 was 5.2 ± 1.6 Gt per year in 1990-2010. Uncertainties stem from the reported 30 % variability be-
124 tween regional climate model results. Note that there is significant variation between models on
125 a sector-by-sector basis.

126 The basal melt due to surface melt water is focussed in areas where surface melt occurs, and
127 where the water is subjected to large hydropotential gradients as it flows along the ice-sheet bed
128 (Fig. 1 F). The basal melt rates are substantially higher than the geothermal basal melt rates along
129 the high-gradient ice-sheet periphery but lower in the interior. The basal melt rates due to surface
130 melt water exceed $5 * 10^{-2}$ m per year in a few places along the margin but the bulk of the sectors

131 have melt rates below 0.5 mm per year. In contrast to the geothermal and frictional terms, the
132 melt due to surface melt water is focused in the conduits and thus highly localised. The values
133 reported above represent an average over 1 km grid cells masking the fact that melt rates vary
134 orders of magnitude over sub-kilometre distances.

135 **Total basal melt on regional and local scales**

136 Our baseline basal melt discharge is estimated at $21.4 +4.4/-4.0$ Gt per year, equivalent to 4.5 % of
137 the annual solid ice discharge (average of 1986–2018 ice discharge[5]). The basal melt also corre-
138 sponds to more than half of the annual discharge of Sermeq Kujalleq (average of 1986–2018), the
139 largest single Greenlandic glacier contributing to sea-level rise[5]. At ice-sheet scale, basal melt is
140 primarily caused by frictional heating (51 %), with surface-melt water heat and geothermal heat
141 as secondary contributors (24 % and 25 %, respectively, Fig. 2B and Table 1). The individual con-
142 tributions from each of the heat terms vary for the different ice-sheet sectors depending on local
143 geothermal flux anomalies and surface melt-water volumes. For example, in the slow-flowing
144 SW sector the relative contributions from the three heat terms approach parity, while friction heat
145 dominates in the CW sector (Table 1).

146 The largest basal mass loss occurs in the CW and SW sector (3.9 ± 0.7 Gt per year), followed by
147 the SE sector ($3.7 +0.8/-0.7$ Gt per year) and the NW sector ($3.5 +0.7/-0.6$ Gt per year). The NO sec-
148 tor has the smallest basal mass loss ($1.5 +0.4/-0.3$ Gt per year) due to a combination of low friction
149 melting and small volumes of surface melt water. The largest mass loss due to surface melt-water
150 heat occurs in the SW sector, while the largest losses due to friction heat and geothermal flux oc-
151 cur in the CW and NE sectors, respectively (Table 1). We note that in order to represent basal
152 mass loss on a sector basis, the subglacial drainage basins are assumed identical to the glacio-
153 logical drainage basins. On drainage-basin scales, we only present the basal melt discharge for
154 three of the largest glaciers (by discharge and flux gate size): Sermeq Kujalleq, which discharges
155 into Qeqertarsuup tunua (Disko Bay), Kangerlussuaq Glacier that discharges into Kangerlussuaq
156 Fjord and Helheim Glacier that terminates in Sermilik Fjord. Here, we calculate the individual
157 subglacial basins using the hydropotential assuming that the subglacial water pressure is at ice
158 overburden pressure[33]. We estimate that at present, the basal melt water flux from Sermeq Ku-
159 jalleq is 1.6 ± 0.5 Gt per year and 41 % of the basal melt water from the CW sector exits through
160 Sermeq Kujalleq into Qeqertarsuup tunua. At Kangerlussuaq Glacier the basal melt discharge is
161 0.8 ± 0.2 Gt per year, corresponding to 35% of the basal melt water in the CE sector. Finally, we find
162 that for Helheim Glacier, the basal melt discharge is 0.9 ± 0.3 Gt per year (24 % of discharge in SE
163 sector).

164 **Temporal evolution of frictional and surface melt-water heat**

165 Above, we reported on a baseline value that represents a multi-decadal average. However, as ice
166 dynamics and surface mass balance respond to changes in climate, by extension the basal-melt
167 contributions from friction heat and surface melt-water heat must also change.

168 The ice sheet underwent a general speed-up during the 2000s[4, 5] and here we investigate
169 its potential effect on the friction melt. In order to obtain annual friction-melt estimates, we need
170 to use a simplified description of the ice dynamics. This is necessary because while Elmer/Ice
171 returns high-resolution insights into the basal melt rates, it comes with substantial computational
172 expense. Instead, we use a simplified approach where the basal sliding is assumed equal to the
173 difference between observed winter surface velocities and deformational (creep) velocities [34]
174 (see methods). We find that the basal melt from our simplified approach is 31% higher compared
175 to the basal melt from the Full Stokes approach. The simplified stress-balance overestimates the
176 basal melt in all sectors (except the CE sector) but the difference is not evenly distributed between
177 sectors with the largest differences in the NE region (59%) and NW sector (52%) (see methods and
178 supplementary materials). In addition to the uncertainty imposed by the simplified stress-balance,
179 other uncertainties include the unknown temperatures of the basal shear layer and the uncertainty
180 from velocity datasets (see methods for a detailed discussion of the uncertainties). Using this
181 simplified approach, we estimate that the friction melt has increased from 10.6 ± 4.3 Gt in winter
182 2000/2001 to 11.8 ± 4.5 Gt in winter 2017/2018, corresponding to an increase of 10 % (Fig. 3). The
183 uncertainty range is mainly due to parameters that are constant in time thus we posit that the
184 reported increase is a consequence of increased ice-flow velocities. A linear regression through
185 the velocity datasets from 2005/2006 through 2017/2018 indicates that basal friction discharge
186 has increased by $0.09 + 0.04 / -0.03$ Gt per year.

187 The surface melt-water volume exhibits high interannual variability and thus constructing a
188 regression line is less meaningful. Instead, we consider the decadal averages 1991-2000 and 2001-
189 2010. We find that basal melt due to surface melt water increased from an average of 3.5 ± 1.1 Gt
190 per year in 1991-2000, to an average of 6.0 ± 1.8 Gt per year in 2001-2010 (Table 2). This corresponds
191 to a 70 % increase in basal melt due to surface melt water. The basal melt for all sectors increased
192 by more than 50 % with the largest increase in the NW sector of 110 %. In order to estimate
193 future change in basal melt due to increased surface melt water, we consider surface melt for 2012.
194 While this was an extreme melt year in the context of present-day melt rates, it is likely that such
195 melt-water volumes will become more common in the future[32]. Using 2012 surface melt water
196 volumes as an analogue of the likely increased future melt, we get basal melt rates of 10 ± 3.0 Gt
197 per year, corresponding to an increase of 4.8 Gt or more than 90%. The largest increase is found
198 in the NE sector (149%) but all sectors experience an increase in basal melt caused by surface melt
199 water (Table 2). In the NE, NO and SW sectors, the basal melt rates from 2012 surface melt water
200 exceed the baseline friction-melt term implying a shift in principal basal melting process. Overall,

201 in the future, basal melt due to heat from surface melt water is likely to become as important as
202 friction melt for ice sheet mass loss.

203 Assuming that the friction-melt term from winter 2000/2001 is representative of the preceding
204 decade, we estimate that the total basal melt production has increased from $19.4 \pm 6.0 / -4.7$ Gt per
205 year in the 1990s to $23.1 \pm 6.1 / -4.9$ Gt per year in the following decade. The change is due to
206 an increase in friction-induced basal melt of 0.4 ± 4.8 Gt (from 10.6 ± 4.3 Gt in winter 2000/2001 to
207 11.0 ± 2.1 Gt (mean of winters 2005/2006 - 2009/2010 using BedMachine topography)), and in basal
208 melt due to surface melt water of 2.5 ± 2.1 Gt. This corresponds to a total increase of 2.9 ± 5.2 Gt.

209 Discussion

210 We have shown that the volume of basal melt water from the Greenland ice sheet can be re-
211 solved and that it is a non-negligible part of the total mass budget. With a total mass balance
212 of -254 ± 18 Gt per year [6], basal melt discharge is presently equivalent to 8 % of this imbalance
213 but is not included in input-output estimates of total mass loss. Basal melt will change as
214 the Greenland ice sheet responds to a warming climate. The frictional heat will increase if the
215 areal extent of the fast-flowing regions expand, leading to an increase in basal melt production.
216 However, the impact of climate change on ice-stream dynamics is complex and thus, we cannot
217 predict by how much the friction term will increase. Based on the recent past (Fig. 3), if glaciers
218 continue to accelerate, basal melt water production may increase by ~ 0.1 Gt every year into the
219 foreseeable future. Heat generated by surface melt water will increase with increasing volumes
220 of surface melt-water production. Under a high-emissions scenario, this melt source will experience
221 a substantial 5-to-7-fold increase by 2100[31]. Thus, the overall mass loss associated with
222 increased surface melt will be further enhanced by the additional basal melt caused by the viscous
223 heat dissipation from the surface melt water.

224 Basal melting may also have a large effect on fjord processes and ice-ocean interaction. During
225 winter, the basal melt discharge that stems from frictional heat and geothermal flux is generated
226 independently of surface melt. Thus, the basal melt introduced and quantified here is the primary
227 source of winter subglacial discharge, and this influx of winter basal water is poorly understood
228 and sparsely measured[35]. Biological productivity is affected by subglacial discharge that modifies
229 mixing in the fjords[12, 36], but the impact of increasing winter freshwater on Arctic fjord
230 environments is as-yet unknown. Studies suggest that winter basal melt discharge may drive
231 year-round submarine meltwater plumes leading to persistent ice-front melting, and that basal
232 melt discharge may pull in warm water from the Atlantic further enhancing frontal melt rates[37].
233 Finally, recent and future increases in basal melting likely have a non-linear effect on ice-sheet
234 discharge. The projected contribution to sea-level rise from the Greenland ice sheet is markedly
235 larger when subglacial discharge is increased, and this effect is comparable to the increase caused

236 by rising ocean temperatures [9]. Thus, an increase in basal melt will likely further compound
237 mass loss from marine-terminating glaciers.

238 **Methods**

239 **Surface and bed topographies**

240 The Elmer/Ice model uses the GIMP digital elevation model (Greenland Ice sheet Mapping Project[38]),
241 and ice thicknesses and bed topography from BedMachine v3 calculated using a mass-conservation
242 method[39].

243 With the simplified stress-balance model, we explore the impact on results using different topogra-
244 phies. Here, estimates are based on two different bed topographies and three different surface
245 elevation datasets. We use the kriging-based bed topography published in 2013[40] and the bed
246 topography from BedMachine v3. Both datasets include a GIMP-derived surface topography that
247 spans a time period between 20 February 2003 to 11 October 2009. In addition, we use the surface
248 topography from the Climate Change Initiative (CCI, <http://cci.esa.int/>) derived from the Arc-
249 ticDEM (Arctic Digital Elevation Model[41]) based mainly on the WorldView 1-3 satellites. This
250 gives a long temporal baseline from 2007 until present day. We combine the CCI surface elevation
251 with the BedMachine v3 bed topography data.

252 For both ice-flow models, we apply an ice cover mask[42] in order to remove local ice caps and
253 glaciers.

254 **Ice velocity data**

255 The inverse method used to tune the basal friction in Elmer/Ice uses a multi-year average of the
256 surface velocity in 250 m resolution from the MEaSURES (Making Earth System Data Records for
257 Use in Research Environments) Greenland Ice Velocity data based on data from RADARSAT-1,
258 ALOS, TerraSAR-X/TanDEM-X and Sentinel-1A and -1B[14, 43].

259 The simple ice-flow model uses two sources for ice velocity: MEaSURES and the PROMICE
260 (Programme for Monitoring of the Greenland ice sheet) velocity product based on Sentinel-1A
261 and -1B[15]. The MEaSURES velocity maps cover the periods from winter 2000/2001 to win-
262 ter 2017/2018 although the coverage is not continuous: Velocity maps are not available from
263 2001/2002 to 2004/2005. Only the latest velocity maps are complete so in order to get better
264 coverage for our estimate of temporal changes we apply the same methodology as described in
265 [5] and linearly interpolate missing values in time. We do not interpolate spatially since spatial
266 changes are most likely larger than temporal changes for any given point. Data at the beginning
267 or end of the time series are back- or forward-filled with the temporally nearest value for that grid
268 cell.

269 The PROMICE dataset spans winter 2016/17 to winter 2018/19 and is based on intensity offset
 270 tracking. Here, the data coverage is near complete and no interpolation is necessary. We note that
 271 the PROMICE maps overestimate the velocities in the interior of the ice sheet where MEaSURES
 272 relies on the more accurate InSAR.

273 Geothermal heat

274 We use the average geothermal flux from three published studies[23, 24, 25]. Note that one of the
 275 datasets (Fox Maule[23]) does not cover the southern tip of Greenland so in this region, the average
 276 geothermal flux map is based on only two datasets ([24] and [24]). We calculate the resulting melt
 277 rates from the geothermal heat assuming that the ice is at pressure melting point[34].

$$\dot{b}_m = \beta \frac{E_b}{\rho_i L} \quad (1)$$

278 where E_b is available energy at the bed, here the geothermal flux, ρ_i is the density of ice, and L
 279 is the latent heat of fusion. The β -parameter indicates the basal conditions. We construct β using
 280 a map of estimated basal conditions based on a combination of radar observations and model
 281 studies[26], where bed conditions were classified as either “likely frozen”, “uncertain” or “likely
 282 thawed”. Here, we assume that $\beta = 0$ where grid cells are assigned as “frozen”, $\beta = 1$ where grid
 283 cells are “thawed”, and $\beta = 0.5$ for all “uncertain” grid cells.

284 Two sources contribute to the uncertainty of our estimate: The uncertainty of the geothermal
 285 flux maps and the unknown basal temperature. We assess the former by considering the spread in
 286 geothermal flux between the maps. Here, we adapt the approach of [44] and define the standard
 287 deviation of the geothermal flux σ_G as

$$\sigma_G = \sigma[G_1 + \delta_1, G_1 - \delta_1, G_2 + \sigma(G_2), G_2 - \sigma(G_2), G_3 + \delta_3, G_3 - \delta_3] \quad (2)$$

288 The uncertainty, δ of the first dataset[45], G_1 , is stated as ranging from 21-27 mW m⁻²[23], where
 289 we choose the higher value. The second dataset[24], G_2 , does not supply an uncertainty and
 290 lacking any other information we use the standard deviation that is given for each data point. The
 291 third dataset[25], G_3 , supplies an uncertainty. We use the standard deviation to calculate the basal
 292 melt from the spread $\bar{G} + \sigma_G$ and $\bar{G} - \sigma_G$, in addition to the basal melt from the mean geothermal
 293 map \bar{G} . This returns an uncertainty of $\pm 21\%$ in total basal melt. On a catchment-scale basis, this
 294 change varies with the largest spread in the SE sector of 34%, while the largest spread in absolute
 295 values is 0.29 Gt per year from the SW sector (see supplementary material).

296 The second uncertainty is the unknown basal temperature of the ice. We continue to make use
 297 of the results from[26] and construct two scenarios: a thawed scenario where we assume that all
 298 regions classified as uncertain are thawed (i.e. we change all areas where $\beta = 0.5$ to $\beta = 1$), and

299 a frozen scenario where we assume that all uncertain regions are frozen (i.e. we change all areas
 300 where $\beta = 0.5$ to $\beta = 0$). We obtain the final uncertainties by considering two end members: 1) a
 301 “warm” scenario where all uncertain areas are assumed to be thawed and where the geothermal
 302 flux equals $\bar{G} + \sigma_G$, and 2) a “cold” scenario where the base is frozen in uncertain areas and where
 303 the geothermal flux is $\bar{G} - \sigma_G$. This gives an upper value of basal melt of 8.1 Gt per year and
 304 a lower value of basal melt of 3.1 Gt per year. Thus, the basal melt due to geothermal flux is 5.3
 305 +2.8/-2.2 Gt per year (see supplementary material for all ranges for each sector and maps showing
 306 the resulting basal melt for the different scenarios considered here).

307 Frictional heat

308 We estimate the frictional heat contribution using two ice-flow models. The Elmer/Ice model is
 309 a Full Stokes model resolving all stresses [29, 30]. The model is inverted in order to minimise the
 310 misfit between modelled and observed surface velocities, where the velocities are a multi-year
 311 velocity mosaic spanning 1995-2015 [13]. The model is computationally expensive which makes it
 312 unfeasible to run an ensemble of models to obtain formal estimates of the uncertainties. Instead,
 313 we investigate the uncertainties associated with our simplified stress-balance model and based on
 314 insights from these experiments, we estimate the uncertainty of the Elmer/Ice output.

315 The second model is a simplified stress-balance equation, the shallow-ice approximation [34], cou-
 316 pled with the velocity observations to calculate the basal sliding velocity. On spatial scales over
 317 several ice thicknesses, ice flow can be assumed to consist of two components: deformational
 318 velocity u_d (at times also referred to as creep velocity) and basal sliding u_b [34]. Thus the total
 319 velocity is

$$u = u_d + u_b \quad (3)$$

320 and here we assume that u is equivalent to the observed surface velocity u_o . Our method thus
 321 retrieves the basal velocity using the observed surface velocity and the calculated deformational
 322 velocity. Theoretically, the surface velocity due to deformation is [34]

$$u_{s,def} = \frac{2A(T)}{n+1} \tau_b^n H \quad (4)$$

323 where $A(T)$ is the flow law parameter, H is ice thickness, n the flow law exponent, and $\tau_b =$
 324 $\tau_d = \rho_i g H \nabla s$, where ρ_i is ice density, g is gravity and ∇s is the surface gradient. We perform this
 325 calculation on a 10 km grid where ice surfaces have been smoothed by a 20 km running mean (in
 326 order to smooth over several ice thicknesses [34]). From the theoretical deformational velocities
 327 we thus get our basal sliding velocity

$$u_b = u_o - u_{s,def} \quad (5)$$

328 and from this we can directly calculate the frictional heat and thereby the melt rate, assuming that
329 the temperature of the ice is at pressure melting point:

$$\dot{b}_m = \frac{u_b \tau_b}{\rho_i L} \quad (6)$$

330 where L is latent heat of fusion of ice at 0°C .

331 The flow law parameter $A(T)$ depends on temperature. Since most of the deformation takes place
332 in the lower 20 % of the ice column, the appropriate value for A in our case is probably closer to the
333 temperature at the bed than the average temperature of the ice column. We use internal ice tem-
334 peratures derived from radar-attenuation values[46] to calculate the deformational velocities, and
335 add a constant offset of 20°C (see supplementary material) to capture temperatures in the lower
336 20 % of the ice column where ice is warmer than the overlying ice[34]. In order to investigate the
337 uncertainties due to poorly constrained internal temperatures, we vary our constant temperature
338 offset by $\pm 5^\circ\text{C}$. We chose $\pm 5^\circ\text{C}$ as a likely uncertainty range because comparison between the in-
339 ternal temperature and estimated basal conditions reveals that changing the offset by more than
340 -5°C returns cold conditions in areas that are likely thawed at the bed[26], while changing the
341 offset by more than $+5^\circ\text{C}$ returns warm conditions in areas that are likely frozen at the bed[26].
342 We find that a change in temperature of $\pm 5^\circ\text{C}$ leads to a change in basal melt from frictional heat
343 by $\mp 25\%$ (for the 2018/2019 velocity dataset).

344 Because we rely on observed velocities to infer the basal sliding, our results are also affected by
345 uncertainties in the velocity data. To translate the velocity uncertainty into friction-melt uncer-
346 tainty, we perturb all points by a randomly selected number between -1 and 1 multiplied with
347 the standard deviation for the point. In this way, we generate 1000 perturbed velocity maps for
348 each MEASUREs dataset from the years 2005/2006, 2007/2008, 2008/2009, 2009/2010, 2012/2013,
349 2014/2015, 2015/2016 and 2016/2017. We then calculate the friction melt for each perturbed ve-
350 locity map and find that this leads to a distribution of friction melt values where 95 % of values
351 deviate less than $\pm 1\%$ from the mean value, and we therefore assign an uncertainty of $\pm 1\%$
352 caused by uncertainties in the velocity datasets.

353 We primarily make use of winter velocities potentially leading to an underestimation of annual
354 basal melt rates since summer velocities are typically higher. We use winter velocities due to the
355 lack of complete maps from summer observations. However, with the recent launch of Sentinel-1,
356 it is possible to construct complete summer velocity maps, and we have included two maps from
357 summers 2018 and 2019. The resulting basal melt rates are 5 % higher for these summer maps
358 likely due to the increased ice-flow velocities. Assuming that summer velocities are representa-
359 tive for at most 50 % of the year, we estimate that exclusively using winter velocities leads to an
360 underestimate of 2.5 %.

361 Due to the simplicity of the shallow-ice approximation, we are also able to explore the impact of
362 using different surface and bed topographies. Using the results from winters 2006/2007, 2007/2008

363 and 2008/2009, we investigate the impact of the difference in topographic datasets. We find that
364 the difference is less than 4 % and typically of the order of 2 % depending on temperature offset.
365 We use 4 % as a conservative upper bound.

366 Assuming that the uncertainties discussed above are independent, we use a simple error propa-
367 gation (square root of the sum of squares) and get an uncertainty of ± 27 %. We assume that this
368 uncertainty range is applicable to both the Elmer/Ice and the shallow-ice approximation models.
369 While Elmer/Ice makes use of temperatures from a paleo spin-up run, its temperature field is still
370 subject to uncertainties, and we consider that a $\pm 5^\circ\text{C}$ uncertainty range is not unlikely.

371 In addition to the uncertainties listed above, studies have shown that deformation predicted by
372 the shallow-ice approximation deviates from observations particularly when sliding is present[47]
373 implying that our predicted basal sliding is incorrect. Furthermore, the shallow-ice approxima-
374 tion limits our horizontal resolution and may not resolve all the narrow (below 20 km wide) and
375 fast flowing outlet glaciers. Comparison with outputs from the Elmer/Ice model shows that the
376 simplified stress-balance leads to an overestimation of basal melt rates of 31 %. Note that in this
377 comparison we use the same temperature and velocity fields in both models so that the difference
378 is mainly due to differences in resolution and stress approximation. The overestimation is partic-
379 ularly pronounced in areas with high surface velocities (e.g., Sermeq Kujalleq) and complex stress
380 regimes (the Northeast Greenland Ice Stream). See also supplementary material for a map high-
381 lighting the differences. The largest differences are found in the NE region (59%) and NW sector
382 (52%), while the difference for other sectors vary between -4% and 38%. Thus, our simple model
383 leads to an overestimation of basal melt rates. We assign a total uncertainty to the values calcu-
384 lated with the shallow-ice approximation of 41 %. Interestingly, recent observations of a borehole
385 in western Greenland found that ice deformation was dominated by sliding in spite of slow ice
386 flow[48]. Our simple analysis infers negligible basal sliding in slow-flowing areas implying that
387 we might be underestimating frictional heat in slow-flowing areas. However, the contribution of
388 basal melt from slow-flowing area is likely orders of magnitudes smaller than the basal melt gen-
389 erated in fast-flowing areas, implying that this underestimation is within our stated uncertainty
390 range.

391 We use the shallow-ice approximation primarily to estimate the change in basal melt, making
392 use of the simplified ice-flow model in order to be able to conduct more model runs. Although
393 the uncertainty of each individual year is 41 %, we postulate that the uncertainty in the change in
394 basal melt is significantly smaller. Below, we outline the reasoning behind this conjecture.

395 We assume that the internal ice temperature is constant in time and thus the uncertainty from the
396 unknown internal temperature is negligible when considering the change in basal melt. We also
397 assume that the uncertainties imposed by the simplified stress balance and the low resolution are
398 constant in time. This assumption is based on the consideration that while the general speed up
399 of the ice sheet should lead to faster and potentially more widespread fast flow, the extent of areas
400 exhibiting complex stress regimes is likely to remain the same, and thus the difference between a

401 Full Stokes calculation and a shallow-ice approximation remains constant.
 402 Instead, uncertainties for the change in friction melt are firstly, based on the difference in slope for
 403 the three temperature offsets (black lines in Fig. 3) and secondly on the uncertainty from the MEa-
 404 SUREs velocity datasets. It should be noted that gaps in the velocity fields typically are back-filled
 405 with data points from later observations where velocities are likely higher, thus we are underesti-
 406 mating the temporal change in basal melt due to the back-filling. Note, that we only use datasets
 407 from years 2005/2006, 2007/2008, 2008/2009, 2009/2010, 2012/2013, 2014/2015, 2015/2016, and
 408 2016/2017 to calculate the regression line shown in Fig. 3 because these datasets have less than
 409 25% of back-filled grid points. The difference in slope for the three temperature offsets can be
 410 found straightforwardly by subtracting the slopes of the regression line. The total uncertainty is
 411 then found with simple error propagation (square root of the sum of squares for the two terms).

412 Subglacial water routing and viscous heat dissipation

413 We estimate the surface melt water contribution using previously published methodology[31]
 414 where heat estimates are derived from runoff values from the GrSMBMIP project (Greenland Sur-
 415 face Mass Balance Model Intercomparison Project). The GrSMBMIP project compiles results from
 416 13 regional climate models during 1980-2012 CE and we use the average values from all 13 mod-
 417 els. The reported spread in modelled surface melt water volumes is 30 % and we use this range as
 418 our uncertainty.

419 We assume that the subglacial water follows the steepest gradient of the hydropotential[33] Φ

$$\Phi = \rho_w g z_b + \rho_i g (z_s - z_b) , \quad (7)$$

420 where ρ_w is the density of water, ρ_i is the density of ice, and z_b and z_s are the elevations of bed and
 421 surface topography, respectively.

422 As the basal melt water travels through the subglacial system it follows the hydropotential gradi-
 423 ent, and energy is released. This energy Q is tracked and depends on the volume of water V , the
 424 change in hydropotential, and the change in phase transition temperature (last term)

$$Q = V \left(\nabla \Phi - C_T c_p \rho_i \rho_w g \nabla (z_s - z_b) \right) , \quad (8)$$

425 where C_T is the Clausius–Clapeyron slope ($8.6 \cdot 10^{-8} \text{ K Pa}^{-1}$), and c_p the specific heat of water
 426 $4184 \text{ J K}^{-1} \text{ kg}^{-1}$.

427 We assume that all potential energy is converted to heat[31], that surface water immediately pene-
 428 trates to the bed and that the englacial water is at the pressure melting point, meaning that the vis-
 429 cous heat dissipation contribution to basal melt is effectively equivalent to the ice volume melted
 430 to form the en- and subglacial conduits[49]. The viscous heat dissipation is the sole reason why
 431 the surface melt water increases the basal melt rates. We also keep track of the energy budget

432 as meltwater enters the hydrological system and melts out channels thus producing additional
433 meltwater. This additional meltwater in turn may melt out more channels in a positive feedback.
434 Lacking information on the exact location of the channels, we assume that they are situated at the
435 bed, and we calculate the potential energy of this additional melt. Locally, this leads to less than
436 1 % increase in basal melt rates.

437 **Data availability**

438 All basal melt maps will be assigned a DOI and made available at the PROMICE website (www.promice.dk)
439 and/or at the GEUS Dataverse website (<https://dataverse01.geus.dk/>). Velocity maps constructed
440 through the PROMICE programme using Sentinel-1 are available at the PROMICE website (www.promice.dk).

441 **Code availability**

442 Code showing examples of how to generate Figures 1D, 1E, 1F and 2A will be posted at the GEUS
443 Dataverse website (<https://dataverse01.geus.dk/>) and the PROMICE GitHub page (<https://github.com/GEUS/PROMICE>).
444 PROMICE).

445 **References**

- 446 [1] Sørensen, L. S. *et al.* Mass balance of the Greenland ice sheet (2003–2008) from ICESat data –
447 the impact of interpolation, sampling and firn density. *The Cryosphere* **5**, 173–186 (2011). URL
448 <https://www.the-cryosphere.net/5/173/2011/>.
- 449 [2] McMillan, M. *et al.* A high-resolution record of Greenland mass balance. *Geophysical Research*
450 *Letters* **43**, 7002–7010 (2016).
- 451 [3] Velicogna, I., Sutterley, T. C. & van den Broeke, M. R. Regional acceleration in ice mass loss
452 from Greenland and Antarctica using GRACE time-variable gravity data. *Geophysical Research*
453 *Letters* **41**, 8130–8137 (2014).
- 454 [4] Mougnot, J. *et al.* Forty-six years of Greenland Ice Sheet mass balance from 1972 to 2018.
455 *Proceedings of the National Academy of Sciences* (2019).
- 456 [5] Mankoff, K. D. *et al.* Greenland Ice Sheet solid ice discharge from 1986 through 2017. *Earth*
457 *System Science Data* **11**, 769–786 (2019).
- 458 [6] Shepherd, A. *et al.* Mass balance of the Greenland Ice Sheet from 1992 to 2018. *Nature* (2019).

- 459 [7] Rignot, E. *et al.* Modeling of ocean-induced ice melt rates of five west Greenland glaciers over
460 the past two decades. *Geophysical Research Letters* **43**, 6374–6382 (2016).
- 461 [8] Jackson, R. H. *et al.* Meltwater Intrusions Reveal Mechanisms for Rapid Submarine Melt
462 at a Tidewater Glacier. *Geophysical Research Letters* **47**, e2019GL085335 (2020). URL
463 <https://agupubs.onlinelibrary.wiley.com/doi/abs/10.1029/2019GL085335>.
- 464 [9] Beckmann, J. *et al.* Modeling the response of Greenland outlet glaciers to global warm-
465 ing using a coupled flow line–plume model. *The Cryosphere* **13**, 2281–2301 (2019). URL
466 <https://www.the-cryosphere.net/13/2281/2019/>.
- 467 [10] Slater, D. A. *et al.* Twenty-first century ocean forcing of the Greenland ice sheet
468 for modelling of sea level contribution. *The Cryosphere* **14**, 985–1008 (2020). URL
469 <https://tc.copernicus.org/articles/14/985/2020/>.
- 470 [11] Meire, L. *et al.* Marine-terminating glaciers sustain high productivity in Green-
471 land fjords, *journal = Global Change Biology* **23**, 5344–5357 (2017). URL
472 <https://onlinelibrary.wiley.com/doi/abs/10.1111/gcb.13801>.
- 473 [12] Hopwood, M. J. *et al.* Review article: How does glacier discharge affect marine biogeochem-
474 istry and primary production in the Arctic? *The Cryosphere* **14**, 1347–1383 (2020).
- 475 [13] Joughin, I., Smith, B. E. & Howat, I. M. A complete map of Greenland ice velocity derived
476 from satellite data collected over 20 years. *Journal of Glaciology* **64**, 1–11 (2018).
- 477 [14] Joughin, I., Smith, B. E., Howat, I. M., Scambos, T. & Moon, T. Greenland flow variability
478 from ice-sheet-wide velocity mapping. *Journal of Glaciology* **56**, 415–430 (2010).
- 479 [15] Solgaard, A. M. & Kusk, A. Programme for monitoring of the
480 Greenland ice sheet (PROMICE): Greenland ice velocity. (2019). URL
481 <http://promice.org/PromiceDataPortal/api/download/92ce7cf4-59b8-4a3f-8f75-93d166f5a7ca/>
- 482 [16] Fettweis, X. *et al.* GrSMBMIP: intercomparison of the modelled 1980–2012 surface mass
483 balance over the Greenland Ice Sheet. *The Cryosphere* **14**, 3935–3958 (2020). URL
484 <https://tc.copernicus.org/articles/14/3935/2020/>.
- 485 [17] Pattyn, F. Investigating the stability of subglacial lakes with a full Stokes ice-sheet model.
486 *Journal of Glaciology* **54** (2008).
- 487 [18] Palmer, S. J. *et al.* Greenland subglacial lakes detected by radar. *Geophysical Research Letters*
488 **40** (2013).
- 489 [19] Bowling, J. S., Livingstone, S. J., Sole, A. J. & Chu, W. Distribution and dynamics of Greenland
490 subglacial lakes. *Nature Communications* **10** (2019).

- 491 [20] Bell, R. E. *et al.* Deformation, warming and softening of Greenland's ice by refreezing melt-
492 water. *Nature Geoscience* (2014).
- 493 [21] Panton, C. & Karlsson, N. B. Automated mapping of near bed radio-echo layer disruptions
494 in the Greenland Ice Sheet. *Earth and Planetary Science Letters* **432**, 323–331 (2015).
- 495 [22] Dow, C. F., Karlsson, N. B. & Werder, M. A. Limited Impact of Subglacial Supercooling
496 Freeze-on for Greenland Ice Sheet Stratigraphy. *Geophysical Research Letters* **45**, 1481–1489
497 (2018).
- 498 [23] Fox Maule, C., Purucker, M. E. & Olsen, N. Inferring magnetic crustal thickness and geother-
499 mal heat flux from crustal magnetic field models (2009).
- 500 [24] Shapiro, N. M. & Ritzwoller, M. H. Inferring surface heat flux distributions guided by a
501 global seismic model: particular application to Antarctica. *Earth and Planetary Science Letters*
502 **223**, 213 – 224 (2004).
- 503 [25] Martos, Y. M. *et al.* Geothermal Heat Flux Reveals the Iceland Hotspot Track Underneath
504 Greenland. *Geophysical Research Letters* **45**, 8214–8222 (2018).
- 505 [26] MacGregor, J. A. *et al.* A synthesis of the basal thermal state of the Greenland Ice Sheet. *Journal*
506 *of Geophysical Research: Earth Surface* **121**, 1328–1350 (2016).
- 507 [27] Fahnestock, M., Abdalati, W., Joughin, I., Brozena, J. & Gogineni, P. High Geothermal Heat
508 Flow, Basal Melt, and the Origin of Rapid Ice Flow in Central Greenland. *Science* **294**, 2338–
509 2342 (2001).
- 510 [28] Smith-Johnsen, S., Schlegel, N.-J., de Fleurian, B. & Nisancioglu, K. H. Sensitivity of the
511 Northeast Greenland Ice Stream to Geothermal Heat. *Journal of Geophysical Research: Earth*
512 *Surface* **125**, e2019JF005252 (2020).
- 513 [29] Gillet-Chaulet, F. *et al.* Greenland ice sheet contribution to sea-level rise from
514 a new-generation ice-sheet model. *The Cryosphere* **6**, 1561–1576 (2012). URL
515 <https://tc.copernicus.org/articles/6/1561/2012/>.
- 516 [30] Maier, N., Gimbert, F., Gillet-Chaulet, F. & Gilbert, A. Basal traction mainly dictated by
517 hard-bed physics over grounded regions of Greenland. *The Cryosphere Discussions* **2020**, 1–31
518 (2020). URL <https://tc.copernicus.org/preprints/tc-2020-185/>.
- 519 [31] Mankoff, K. D. & Tulaczyk, S. M. The past, present, and future viscous heat dissipation
520 available for Greenland subglacial conduit formation. *The Cryosphere* **11**, 303–317 (2017). URL
521 <https://www.the-cryosphere.net/11/303/2017/>.

- 522 [32] Fettweis, X. *et al.* Estimating the Greenland ice sheet surface mass balance contribution to
523 future sea level rise using the regional atmospheric climate model MAR. *The Cryosphere* **7**,
524 469–489 (2013). URL <https://www.the-cryosphere.net/7/469/2013/>.
- 525 [33] Shreve, R. L. Movement of Water in Glaciers. *Journal of Glaciology* **11**, 205–214 (1972).
- 526 [34] Cuffey, K. M. & Paterson, W. S. B. *The Physics of Glaciers* (Butterworth-Heinemann, 2010).
- 527 [35] Pitcher, L. H. *et al.* Direct Observation of Winter Meltwater Drainage From the Greenland Ice
528 Sheet. *Geophysical Research Letters* **47**, e2019GL086521 (2020).
- 529 [36] Vonnahme, T. R. *et al.* Subglacial upwelling in winter/spring increases under-
530 ice primary production. *The Cryosphere Discussions* **2020**, 1–45 (2020). URL
531 <https://tc.copernicus.org/preprints/tc-2020-326/>.
- 532 [37] Cook, S. J., Christoffersen, P., Todd, J., Slater, D. & Chauché, N. Coupled modelling of sub-
533 glacial hydrology and calving-front melting at Store Glacier, West Greenland. *The Cryosphere*
534 **14**, 905–924 (2020). URL <https://www.the-cryosphere.net/14/905/2020/>.
- 535 [38] Howat, I. M., Negrete, A. & Smith, B. E. The Greenland Ice Mapping Project (GIMP) land
536 classification and surface elevation data sets. *The Cryosphere* **8**, 1509–1518 (2014). URL
537 <https://www.the-cryosphere.net/8/1509/2014/>.
- 538 [39] Morlighem, M. *et al.* BedMachine v3: Complete Bed Topography and Ocean Bathymetry
539 Mapping of Greenland From Multibeam Echo Sounding Combined With Mass Conservation.
540 *Geophysical Research Letters* **44**, 11,051–11,061 (2017).
- 541 [40] Bamber, J. L. *et al.* A new bed elevation dataset for Greenland. *The Cryosphere* **7**, 499–510
542 (2013).
- 543 [41] Porter, C. *et al.* ArcticDEM (2018). URL <https://doi.org/10.7910/DVN/OHHUKH>.
- 544 [42] Citterio, M. & Ahlstrøm, A. P. Brief communication “the aerophotogrammet-
545 ric map of Greenland ice masses”. *The Cryosphere* **7**, 445–449 (2013). URL
546 <https://www.the-cryosphere.net/7/445/2013/>.
- 547 [43] Howat, I. MEaSURES Greenland Ice Velocity: Selected Glacier Site Veloc-
548 ity Maps from Optical Images, Version 2. 0478, updated 2019. (2019). URL
549 <https://nsidc.org/data/NSIDC-0646/versions/2>.
- 550 [44] Van Liefferinge, B. & Pattyn, F. Using ice-flow models to evaluate potential sites of million
551 year-old ice in Antarctica. *Climate of the Past* **9**, 2335–2345 (2013).

- 552 [45] Fox Maule, C., Purucker, M. E., Olsen, N. & Mosegaard, K. Heat Flux Anomalies in Antarctica
553 Revealed by Satellite Magnetic Data. *Science* **309**, 464–467 (2005).
- 554 [46] MacGregor, J. A. *et al.* Radar attenuation and temperature within the Green-
555 land Ice Sheet. *Journal of Geophysical Research: Earth Surface* **120**, 983–1008
556 (2015). URL <https://agupubs.onlinelibrary.wiley.com/doi/abs/10.1002/2014JF003418>.
557 <https://agupubs.onlinelibrary.wiley.com/doi/pdf/10.1002/2014JF003418>.
- 558 [47] Ryser, C. *et al.* Sustained high basal motion of the Greenland ice sheet revealed by borehole
559 deformation. *Journal of Glaciology* **60**, 647–660 (2014).
- 560 [48] Maier, N., Humphrey, N., Harper, J. & Meierbachtol, T. Sliding dominates slow-
561 flowing margin regions, Greenland Ice Sheet. *Science Advances* **5** (2019). URL
562 <https://advances.sciencemag.org/content/5/7/eaaw5406>.
- 563 [49] Isenko, E., Naruse, R. & Mavlyudov, B. Water temperature in englacial and
564 supraglacial channels: Change along the flow and contribution to ice melting on
565 the channel wall. *Cold Regions Science and Technology* **42**, 53 – 62 (2005). URL
566 <http://www.sciencedirect.com/science/article/pii/S0165232X04001594>.
- 567 [50] Mouginot, J. & Rignot, E. Glacier catchments/basins for the Greenland Ice Sheet (2019).

568 **Acknowledgements**

569 PROMICE is funded by the Geological Survey of Denmark and Greenland (GEUS) and the Dan-
570 ish Ministry of Climate, Energy and Utilities under the Danish Cooperation for Environment in
571 the Arctic (DANCEA), and is conducted in collaboration with DTU Space (Technical University
572 of Denmark) and Asiaq, Greenland. The authors gratefully acknowledge insights from S. Rys-
573 gaard (Aarhus University, Denmark) and M. Oksman (GEUS) on marine nutrients and primary
574 production.

575 **Author contributions statement**

576 N.B.K. conceived the study in collaboration with A.M.S, D.I.B. and I.H. N.B.K. designed and ran
577 the models. A.M.S. constructed the velocity data sets, K.D.M. calculated the surface melt water
578 contribution. F.G.-C. provided Elmer/Ice outputs. J.A.M. provided internal and basal temperature
579 maps. J.E.B. contributed to discussions of total mass balance. M.C. adapted an ice mask for the
580 purposes of this study. S.H.L. assisted with error checking the code. W.T.C., R.S.F. and K.K.K.
581 compiled mass budget information for comparison. N.J.K. assisted with figures. N.B.K. wrote the
582 manuscript with input from all authors.

Sector	Geothermal (Gt per year)	Friction (Gt per year)	Surface water (Gt per year)	Total melt (Gt per year)
Central east (CE)	0.5 +0.5/-0.3	1.2±0.3	0.5±0.2	2.3 +0.6/-0.5
Central west (CW)	0.7 +0.3/-0.2	2.4±0.6	0.7±0.2	3.9 +0.7/-0.7
Northeast (NE)	1.3 +0.6/-0.5	1.0±0.3	0.5±0.1	2.8 +0.7/-0.6
North (NO)	0.4 +0.3/-0.3	0.6±0.2	0.4±0.1	1.5 +0.4/-0.3
Northwest (NW)	0.6 +0.2/-0.2	2.1±0.6	0.8±0.3	3.5 +0.7/-0.6
Southeast (SE)	0.7 +0.5/-0.3	2.2±0.6	0.8±0.3	3.7 +0.8/-0.7
Southwest (SW)	1.2 +0.4/-0.4	1.3±0.4	1.4±0.4	3.9 +0.7/-0.7
Total	5.3 +2.8/-2.2	10.9±3.0	5.2±1.6	21.4 +4.4/-4.0

Table 1: Basal melt from the three heat terms and the total basal melt. The friction heat term is based on ice-velocity data spanning 1995-2015 while the surface melt-water heat term spans 1995-2010.

Sector	Surface water 1991-2000 (Gt per year)	Surface water 2001-2010 (Gt per year)	Surface water 2012 (Gt per year)
Central east (CE)	0.4±0.1	0.6±0.2	0.9±0.3
Central west (CW)	0.5±0.2	0.8±0.3	1.4±0.4
Northeast (NE)	0.3±0.09	0.6±0.2	1.2±0.3
North (NO)	0.3±0.08	0.5±0.1	0.9±0.3
Northwest (NW)	0.5±0.1	1.0±0.3	1.6±0.5
Southeast (SE)	0.6±0.2	0.9±0.3	1.4±0.4
Southwest (SW)	1.0±0.3	1.5±0.5	2.6±0.8
Total	3.5±1.1	6.0±1.8	10.0±3.0

Table 2: Basal melting in Gt per year due to surface melt-water heat for decadal averages 1991-2000 and 2001-2010, and for 2012. Note the substantially higher melt in 2012 due to large volumes of melt water.

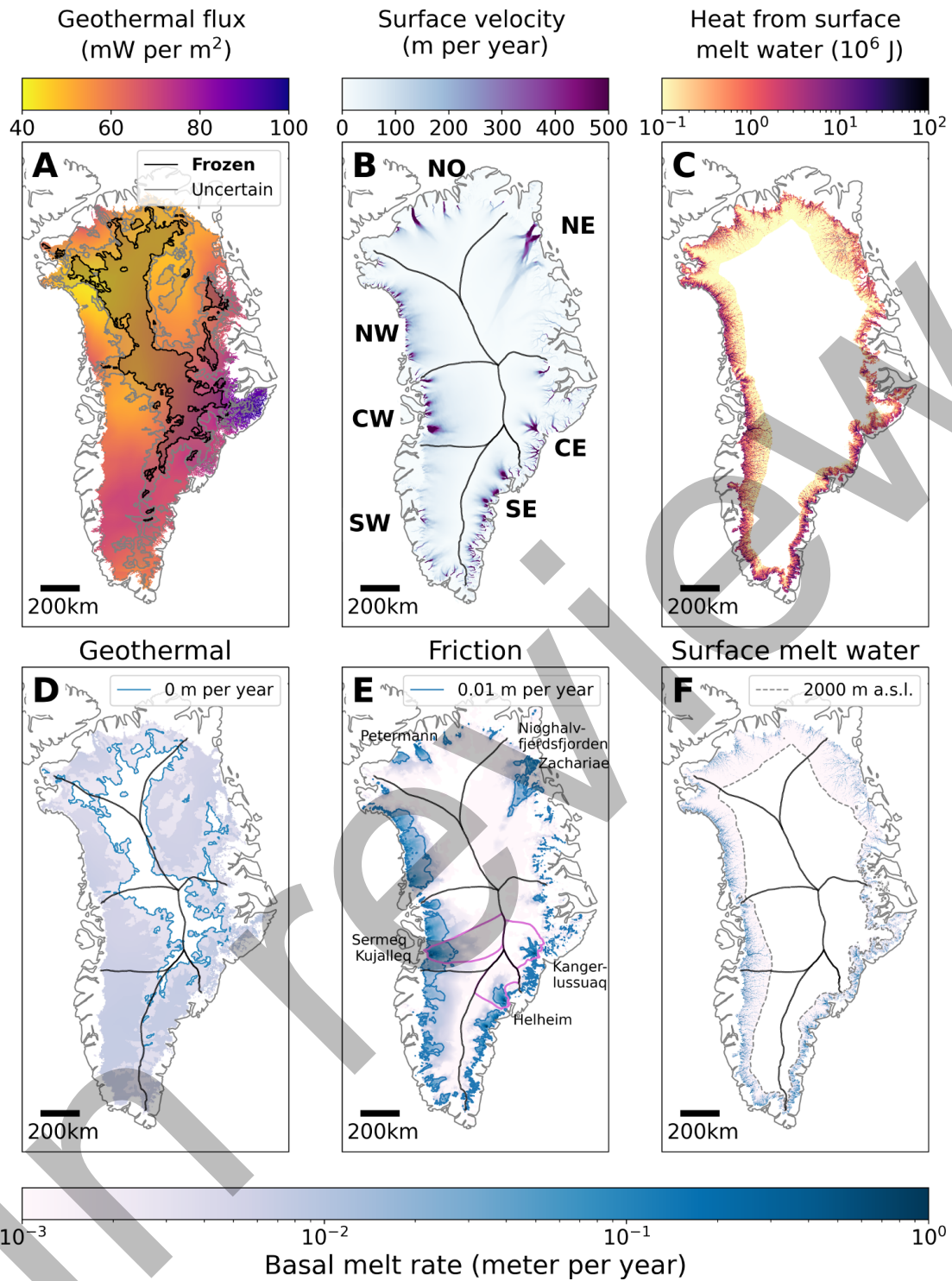


Figure 1: (A) Mean geothermal flux from [23, 24, 25]. The shaded areas outline where bed conditions are likely frozen (black) or uncertain (gray) based on radar observations and numerical ice-flow models[26]. (B) Surface velocities from multi-year MEaSURES dataset[13]. (C) Heat generated by surface melt-water infiltration. (D) Basal melting from geothermal heating. Blue contours outline the 0 m per year extent. (E) Basal melting from frictional heating. Purple outlines show the glacial catchments of Sermeq Kujalleq, Kangerlussuaq and Helheim Glacier[50]. Blue contours outline the 10^{-2} m per year extent. (F) Basal melting from surface water heating. Dashed gray contours outline the 2000 m above sea level elevation. (D), (E), and (F) have the same logarithmic scalebar.

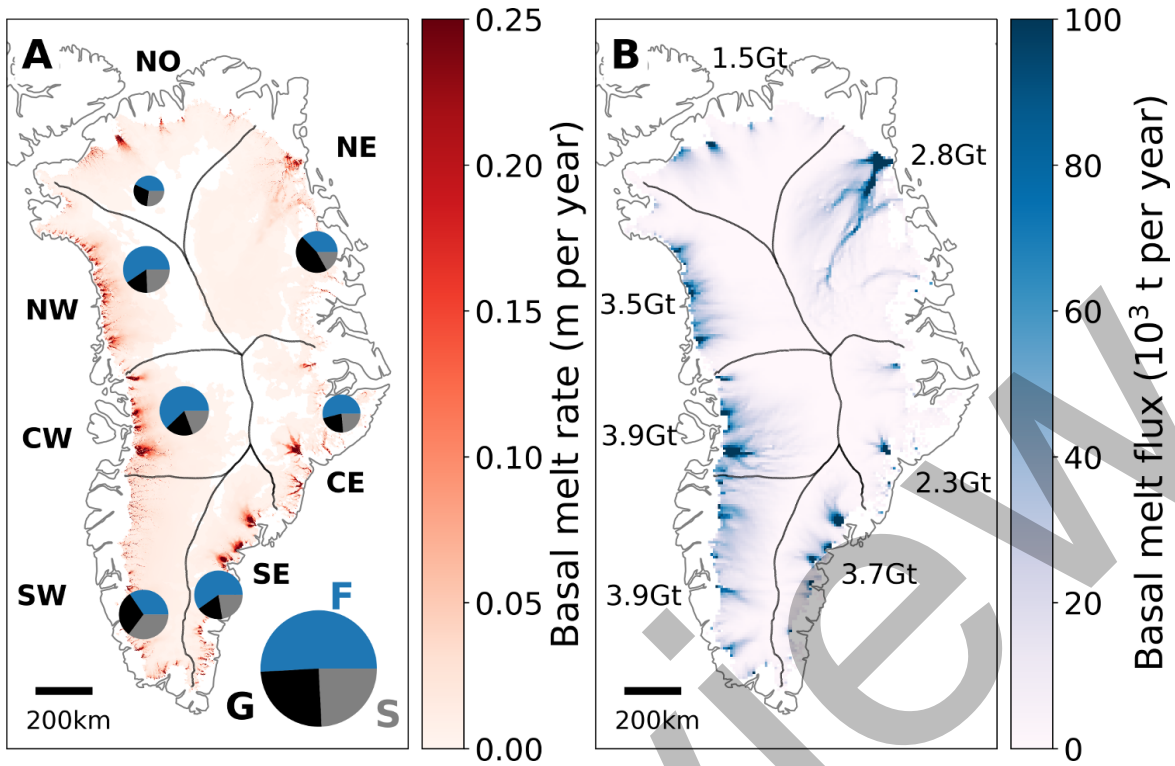


Figure 2: (A) Basal melt rates. Pie charts show the contribution from the different heat terms: friction heat (F, blue), geothermal flux (G, black) and viscous heat dissipation from surface melt water (S, grey). Size of circles indicate the total basal melt discharge from each sector. (B) Flux of basal melt water. Numbers show the total basal melt discharge for each sector.

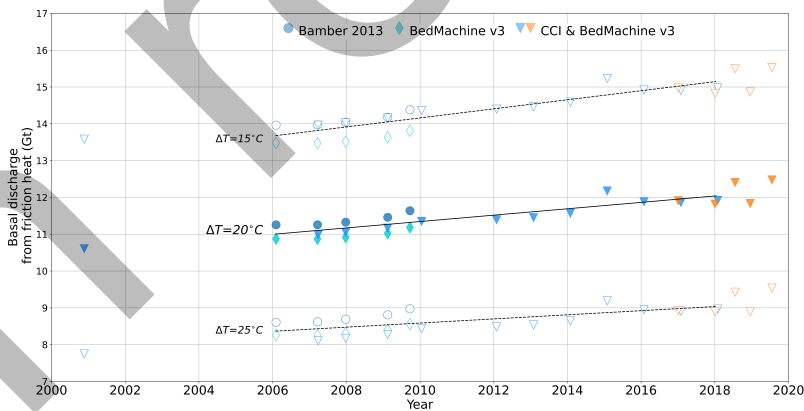


Figure 3: Basal melt discharge due to friction heat from winter 2000/2001 through to winter 2018/2019. Blue and turquoise colours indicate results based on the gap-filled MEaSUREs dataset (see methods). Orange colours indicate that results are from the PROMICE Sentinel-1 derived velocities. Black line is best linear fit through the MEaSUREs datasets (from the years 2005/2006, 2007/2008, 2008/2009, 2009/2010, 2012/2013, 2014/2015, 2015/2016 and 2016/2017), dashed black lines represent best linear fit if internal ice deformation temperatures are offset by $\pm 5^\circ\text{C}$. The shape of the points indicate origin of surface and bed topographies.